Registration of Multichannel Images using Geometric Algebra

Andreas Görlitz
Darmstadt University of Technology
Department of Computer Science
Hochschulstr. 10
64289 Darmstadt, Germany

A.Goerlitz@stud.tu-darmstadt.de

Helmut Seibert
Fraunhofer Institute for
Computer Graphics Research
Fraunhoferstr. 5
64283 Darmstadt, Germany

helmut.seibert@igd.fraunhofer.de

Dietmar Hildenbrand
Darmstadt University of Technology
Department of Computer Science
Hochschulstr. 10
64289 Darmstadt, Germany

dhilden@gris.informatik.tu-darmstadt.de

ABSTRACT

Geometric Algebra (GA) is a mathematical framework that allows a compact and geometrically intuitive description of geometric relationships and algorithms. In this paper a translation, rotation and scale invariant algorithm for registration of color images and other multichannel data is introduced. The use of Geometric Algebra allows to generalize the well known Fourier Transform which is widely used for the registration of scalar fields. In contrast to the original algorithm our algorithm allows to handle vector valued data in an appropriate way. As a proof of concept the registration results for artificial, as well as for real world data, are discussed.

Keywords

Registration, Multichannel Images, Color Images, Clifford Fourier Transform, Geometric Algebra (GA)

1 INTRODUCTION

Registration of images is a crucial step in many image processing applications where the final information is obtained by combining multiple input images. Widely used applications such as image stitching [16], medical imaging [3] and video tracking [15], heavily rely on the accuracy of image registration. A broad variety of approaches for various image registration problems has been developed and presented in the literature, a survey which classifies the different approaches is given in [19].

In many applications multi-channel images are available, which require adequate processing of vector data. Fundamental image processing steps such as convolution and correlation are not well suited to work with vector data, as the multiplication of vectors has a different meaning as the multiplication of scalar values. In practice there are two common ways to work around this limitation. One is to reduce the dimensionality, e.g. to convert color images to a monochrome representation. The other way is to handle the vector components respective channels independently and to combine the results afterwards, e.g. perform a filter operation on the red, green, and blue channel of a RGB image separately.

Obviously both approaches cause inaccuracies by introducing information loss or misinterpretations and may lead to inappropriate results.

The key innovation of our work presented here is a way to perform a registration of multichannel images based on the Fourier Transform using Geometric Algebra as an adequate mathematic foundation to handle vector data in a well defined and appropriate way.

In Section 3 a brief introduction of some Geometric Algebra basics is given and the registration of images using the Fourier Transform is discussed. As main contribution of this paper the generalization of this registration approach for multichannel images, such as color images, introduced in Section 4. The evaluation and the results are discussed in Section 5 and 6 respectively, and afterwards a conclusion is given in Section 7. Finally an outlook to the future work is given in Section 8.

2 RELATED WORK

Applications that rely on registration of images are a.o.: image stitching [16], medical imaging [3] and video tracking [15]. Especially in medical imaging the registration of multichannel images plays an important role [12], [14]. To be able to process these multichannel images in the phase domain, a generalization of the classical Fourier-Transform is needed. Many different approaches have been invented to generalize the classical Fourier Transform in the recent years [2], [7] and [8]. The basis of this paper is the so called Clifford-Fourier-Transform that was derived and successfully used in [5] and [6].

3 PREREQUISITES

3.1 Geometric Algebra

Below we only describe the parts of the *Geometric Algebra* on $\mathbb{R}^n$, $\mathcal{G}(\mathbb{R}^n)$ or in abbreviate form $\mathcal{G}_n$, that will be used in this paper. For a more detailed introduction to Geometric Algebra we reference to [1], [4], [11], [18].

Inner Product: let $\mathbf{a}, \mathbf{b}, \mathbf{c} \in \mathcal{G}_n$ be Geometric Algebra vectors and $k \in \mathbb{R}$, then the inner product $\mathbf{a} \cdot \mathbf{b}$, that is also known as the *scalar product* from vector calculus, has the following properties:

$$\mathbf{a} \cdot \mathbf{b} = \mathbf{b} \cdot \mathbf{a}$$
$$(k\mathbf{a}) \cdot \mathbf{b} = k(\mathbf{a} \cdot \mathbf{b})$$
$$\mathbf{a} \cdot (\mathbf{b} + \mathbf{c}) = \mathbf{a} \cdot \mathbf{b} + \mathbf{a} \cdot \mathbf{c} .$$

Further we also know from vector calculus that $\mathbf{a} \cdot \mathbf{b} = |\mathbf{a}||\mathbf{b}|\cos(\alpha)$, where α is the angle between $\mathbf{a}$ and $\mathbf{b}$, i.e. $\mathbf{a} \cdot \mathbf{b} = 0 \quad \mathbf{a}, \mathbf{b} \neq 0 \Leftrightarrow \mathbf{a}$ and $\mathbf{b}$ are orthogonal.

Outer Product: let $\mathbf{a}, \mathbf{b}, \mathbf{c} \in \mathcal{G}_n$ be Geometric Algebra vectors and $k \in \mathbb{R}$, then the outer product $\mathbf{a} \wedge \mathbf{b}$ has the following properties:

$$\mathbf{a} \wedge \mathbf{b} = -\mathbf{b} \wedge \mathbf{a}$$
$$(\mathbf{a} \wedge \mathbf{b}) \wedge \mathbf{c} = \mathbf{a} \wedge (\mathbf{b} \wedge \mathbf{c})$$
$$\mathbf{a} \wedge (\mathbf{b} + \mathbf{c}) = \mathbf{a} \wedge \mathbf{b} + \mathbf{a} \wedge \mathbf{c}$$
$$(k\mathbf{a}) \wedge \mathbf{b} = k(\mathbf{a} \wedge \mathbf{b}) .$$

It can be shown that the outer product $\mathbf{a} \wedge \mathbf{b}$ spans a plane, i.e. $\mathbf{a} \wedge \mathbf{b} = 0 \Leftrightarrow \mathbf{a}$ and $\mathbf{b}$ are parallel.

A term like $\bigwedge_{i=1}^{k} b_i = b_1 \wedge b_2 \wedge \cdots \wedge b_k$ is being called a *k-blade*. A *unit n-blade* is often referred to as a *pseudoscalar* $e_1 \wedge e_2 \wedge \cdots \wedge e_n = \mathbf{i}_n$, where e_i are *unit vectors*, i.e. $e_i \cdot e_j = \delta_{ij}$.

Geometric Product: let $\mathbf{a}, \mathbf{b}, \mathbf{c} \in \mathcal{G}_n$ be Geometric Algebra vectors, then the geometric product $\mathbf{ab}$ is simply the sum of the inner and outer product $\mathbf{ab} = \mathbf{a} \cdot \mathbf{b} + \mathbf{a} \wedge \mathbf{b}$ with the properties:

$$(\mathbf{ab})\mathbf{c} = \mathbf{a}(\mathbf{bc})$$
$$\mathbf{a}(\mathbf{b} + \mathbf{c}) = \mathbf{ab} + \mathbf{ac}$$
$$(\mathbf{b} + \mathbf{c})\mathbf{a} = \mathbf{ba} + \mathbf{ca} .$$

The sum of scalars, vectors and blades is denoted as *multivector*, especially every single scalar, vector and blade is a multivector too, i.e. the result of any afore mentioned product is a *multivector* in general.

Rotations in $\mathcal{G}_n$: let $e_1, e_2, \ldots, e_n$ be unit vectors in $\mathcal{G}_n$, then with $i \neq j$

$$(e_i \wedge e_j)(e_i \wedge e_j) = -1 , \tag{1}$$

a proof is given in Appendix A.1.

So, similar to *Euler's Formula*, by substituting $e_1 \wedge e_2 = i$, where i is the imaginary unit, and computing *Taylor series expansion* of $exp(\phi(e_1 \wedge e_2))$, or in shorthand notation $e^{\phi(e_1 \wedge e_2)}$, we get

$$e^{\phi(e_1 \wedge e_2)} = \cos(\phi) + (e_1 \wedge e_2)\sin(\phi) , \tag{2}$$

which is the well known rotation operator (rotor) for complex numbers.

Unlike the case of complex numbers, for a general rotation in $\mathcal{G}_n$ of an arbitrary plane $L = \sum_{i=1}^{n} \sum_{j=i+1}^{n} k_{ij} e_i \wedge e_j$ with $0 \leq k_{ij} \leq 1$ and $\sum_{i,j} k_{ij} = 1$ a two-sided rotor is needed

$$\mathbf{a}_{rotated} = e^{\frac{-\phi}{2}L} \, \mathbf{a} \, e^{\frac{\phi}{2}L} . \tag{3}$$

This is given by the fact that a two-sided rotor has no effect on vectors perpendicular to the rotation plane, e.g.

$$e^{\frac{-\phi}{2}e_1 \wedge e_2} \, e_3 \, e^{\frac{\phi}{2}e_1 \wedge e_2} = e_3 . \tag{4}$$

a proof is given in Appendix A.2. A one-sided rotor does not have this property.

3.2 Fourier-Mellin Transform

In this Section we briefly introduce the application of the Fourier-Mellin Transform for registration of grayscaled images. All theorems and proofs according to the Fourier-Transform can be found in [10].

As in [10], we use the following definition of the Fourier-Transform of a function $f : \mathbb{R}^2 \to \mathbb{C}^2$

$$F(\chi, \xi) = \int_{-\infty}^{+\infty} \int_{-\infty}^{+\infty} f(x,y) e^{-2\pi i(\chi x + \xi y)} dxdy ,$$

and the Inverse Fourier-Transform as

$$\hat{f}(x,y) = \int_{-\infty}^{+\infty} \int_{-\infty}^{+\infty} F(\chi, \xi) e^{-2\pi i(\chi x + \xi y)} d\chi d\xi .$$

Translation Invariance: let f_1 and f_2 be two images with the following relation:

$$f_1(x,y) = f_2(x - t_x, y - t_y) , \tag{5}$$

i.e. moving f_2 by t_x (right) and t_y (down) will result in f_1. Further let F_1 and F_2 be the Fourier-Transforms of f_1 respective f_2, then by the shift-theorem both are related to each other by:

$$F_1(\chi, \gamma) = F_2(\chi, \gamma) e^{-2i\pi(\chi t_x + \gamma t_y)} , \tag{6}$$

where i is the imaginary unit.

The latter equation can be rearranged to:

$$\frac{F_2^*(\chi, \gamma) F_1(\chi, \gamma)}{|F_2(\chi, \gamma)|^2} = e^{-2i\pi(\chi t_x + \gamma t_y)} , \tag{7}$$

where $F_2^*(\chi, \gamma)$ denotes the conjugate complex Value of $F_2(\chi, \gamma)$.

The right-hand side of (7) is a Fourier-Transform of the Dirac-Delta function[1], i.e.:

$$e^{-2\pi i(\chi t_x + \gamma t_y)} = \iint_{\mathbb{R}^2} \delta(x - t_x, y - t_y) e^{-2\pi i(\chi x + \gamma y)} dxdy .$$

Since the inverse Fourier-Transform gives us the Dirac Delta function $\delta(x - t_x, y - t_y)$, the position of the Dirac impulse gives us the values for t_x and t_y, as can be seen in Figure 1.

---

[1] or to be more precise *Dirac Delta distribution*

<div align="center">(a)   (b)   (c)</div>

Figure 1: According to Paragraph *Translation Invariance* in Section 3.2, (a) is f_1 and (b) is f_2 with the relation $f_1(x,y) = f_2(x-50, y-10)$, which means that shifting (b) 50 pixels right and 10 pixels down will result in (a) (the origin is the upper left corner and the image sizes are 128×128). The *Inverse Fourier Transform* of the left-hand side of equation (7) results in (c). The *Dirac Impulse* p, i.e. the white point, has got the coordinates $p = (50, 10)^T$.

Rotation and Scale Invariance: let f_1 and f_2 be two images with the following relation:

$$f_1(x,y) = f_2(x\cos(\alpha) + y\sin(\alpha), y\cos(\alpha) - x\sin(\alpha)) \ , \quad (8)$$

i.e. rotating f_2 by the angle α will result in f_1. Transforming from Cartesian (x,y) to polar coordinates, the latter equation can be written as:

$$f_1 = f_2(r, \phi - \alpha) \ ,$$

and is syntactically similar to equation (5) now. So the value for α can be computed in the same way as explained previously.

Having not only a difference in rotation but also in all directions equal scale, one gets

$$f_1(x,y) = f_2(\frac{x}{s}\cos(\alpha) + \frac{y}{s}\sin(\alpha), \frac{y}{s}\cos(\alpha) - \frac{x}{s}\sin(\alpha)) \ ,$$

where s is the so called scaling factor.

Transforming both sides of the above equation to polar coordinates results in

$$f_1(r, \phi) = f_2(\frac{r}{s}, \phi - \alpha) \ .$$

Computing the logarithm of $\frac{r}{s}$ gives the so called *log-polar coordinates* which leads to

$$f_1(\log(r), \phi) = f_2(\log(r) - \log(s), \phi - \alpha) \ , \quad (9)$$

the same structure as in (5), so that α and $\log(s)$, respective the scaling factor s, can be computed as described above.

The Fourier-Transform F^l of $f(x,y)$ in log-polar coordinates can be rearranged as follows:

$$
\begin{aligned}
F^l(u_1, u_2) &= \int_0^{2\pi} \int_0^{+\infty} f(\log(r), \phi) e^{-2\pi i(u_1\log(r) + u_2\phi)} \mathrm{d}\log(r)\mathrm{d}\phi \\
&= \int_0^{2\pi} \int_0^{+\infty} f(\log(r), \phi) r^{-2\pi i u_1} e^{-2\pi u_2\phi} \mathrm{d}\log(r)\mathrm{d}\phi \\
&= \int_0^{2\pi} \int_0^{+\infty} f(\log(r), \phi) r^{-2\pi i u_1 - 1} \mathrm{d}r e^{-2\pi u_2\phi} \mathrm{d}\phi \ .
\end{aligned}
$$

Since the inner integral is a Mellin-Transform while the outer integral is a Fourier-Transform, the whole formula is often referred to as the *Fourier Mellin Transform*.

Translation, Rotation and Scale Invariance: let f_1 and f_2 be two images, with the relation

$$f_1(x,y) = f_2(sx\cos(\alpha) + sy\sin(\alpha) - t_x, sy\cos(\alpha) - sx\sin(\alpha) - t_y) \ ,$$

i.e. rotating f_2 by the angle α, scaling by $s > 0$ and finally shifting it by t_x and t_y will result in f_1 .

The Fourier-Transforms of both sides are related to each other by

$$F_1(\chi, \gamma) = F_2\left(\frac{\chi\cos(\alpha) + \gamma\sin(\alpha)}{a}, \frac{\gamma\cos(\alpha) - \chi\sin(\alpha)}{a}\right)\frac{e^{-2\pi i(\chi t_x + \gamma t_y)}}{a^2} \ .$$

The factor $e^{-2\pi i(\chi t_x + \gamma t_y)}$ is a rotor, i.e. it changes only the orientation but not the magnitudes of F_2. So computing the magnitude spectra M_1, M_2 of F_1 and F_2 leads to

$$M_1(\chi, \gamma) = M_2\left(\frac{\chi\cos(\alpha) + \gamma\sin(\alpha)}{s}, \frac{\gamma\cos(\alpha) - \chi\sin(\alpha)}{s}\right)\frac{1}{s^2} \ .$$

Fourier-Mellin Transforming both sides in log-polar coordinates results in

$$F_{M_1}(\xi, \psi) = F_{M_2}(\xi, \psi)\frac{e^{-2\pi i(\xi s + \psi\alpha)}}{s^2} \ .$$

Now computing the magnitudes of both sides leads to

$$M_{F_{M_1}}(\xi, \psi) = M_{F_{M_2}}(\xi, \psi)\frac{1}{s^2} \ , \quad (10)$$

that finally can be rearranged to

$$s = \sqrt{\frac{M_{F_{M_1}}(\xi, \psi)}{M_{F_{M_2}}(\xi, \psi)}} \ . \quad (11)$$

Having the value of s we are able to compute the value of α as described in *Scale and Rotation Invariance* and subsequent the values for t_x and t_y as described in *Translation Invariance*.

4 GENERALIZED REGISTRATION

In this Section we generalize the method of registering grayscaled images as mentioned above, to a method that allows a registration of multichannel images as well. Therefore we make use of the Geometric Algebra and the *Clifford Fourier Transform* (CFT) introduced in [6] that is defined as

$$\mathbf{F}(\chi) = \int_{\mathbb{R}^n} \mathbf{f}(\mathbf{x}) e^{-2\pi \mathbf{i}_n(\mathbf{x}\cdot\chi)} d\mathbf{x} \; , \qquad (12)$$

and its inverse

$$\bar{\mathbf{f}}(\mathbf{x}) = \int_{\mathbb{R}^n} \mathbf{F}(\chi) e^{-2\pi \mathbf{i}_n(\mathbf{x}\cdot\chi)} d\xi \; , \qquad (13)$$

where $\mathbf{x}, \xi \in \mathbb{R}^n$ are two n dimensional vectors, $\mathbf{i}_n$ is a *pseudoscalar*, i.e. $\mathbf{i}_n\mathbf{i}_n = -1$ (the proof is analogous to the one given in Appendix A.1), and $\mathbf{f}, \bar{\mathbf{f}}: \mathbb{R}^n \to \mathcal{G}_m$ are multivector valued signals.

The main advantage of this Fourier Transform is that it is a sum of classical Fourier Transforms,

$$
\begin{aligned}
\mathbf{F}(\chi) &= \int_{\mathbb{R}^n} \mathbf{f}(\mathbf{x}) e^{-2\pi \mathbf{i}_n(\mathbf{x}\cdot\chi)} d\mathbf{x} \\
&= \int_{\mathbb{R}^n} (f_1(\mathbf{x})e_1 + f_2(\mathbf{x})e_2 + \cdots + f_n(\mathbf{x})e_n)\, e^{-2\pi \mathbf{i}_n(\mathbf{x}\cdot\chi)} d\mathbf{x} \\
&= \int_{\mathbb{R}^n} (-1)^{n-1} f_1(\mathbf{x}) e^{-2\pi \mathbf{i}_n(\mathbf{x}\cdot\chi)} e_1 \\
&\quad + (-1)^{n-1} f_2(\mathbf{x}) e^{-2\pi \mathbf{i}_n(\mathbf{x}\cdot\chi)} e_2 \\
&\quad + \cdots + (-1)^{n-1} f_n(\mathbf{x}) e^{-2\pi \mathbf{i}_n(\mathbf{x}\cdot\chi)} e_n\, d\mathbf{x} \\
&= (-1)^{n-1} F_1(\mathbf{x}) e_1 + \cdots + (-1)^{n-1} F_n(\mathbf{x}) e_n \; , \quad (14)
\end{aligned}
$$

i.e. high-performance implementations can be realized by using Fast Fourier Transforms.

4.1 Translation Invariance

Let $\mathbf{f}_1, \mathbf{f}_2 : \mathbb{R}^n \to \mathbb{R}^m$ be two vector valued signals and let $\mathbf{x}, \mathbf{t} \in \mathbb{R}^n$ with the following relation:

$$\mathbf{f}_1(\mathbf{x}) = \mathbf{f}_2(\mathbf{x} - \mathbf{t}) \; .$$

The Fourier Transforms $\mathbf{F}_1, \mathbf{F}_2$ of $\mathbf{f}_1$ and $\mathbf{f}_2$ respectively are related by

$$\mathbf{F}_1(\chi) = \mathbf{F}_2(\chi) e^{-2\pi \mathbf{i}_n(\mathbf{t}\cdot\chi)} \; , \qquad (15)$$

a proof is given in Appendix A.3.

Analogously to the afore mentioned case for grayscaled images, multiplying the inverse of $\mathbf{F}_2$ from the left and computing the inverse Clifford Fourier Transform (13) will result in the Dirac Delta function $\delta(\mathbf{x} - \mathbf{t})$, i.e. the impulse is located at position $\mathbf{t} \in \mathbb{R}^n$. A proof is given in A.4.

4.2 Rotation and Scale Invariance

As described in paragraph *Rotations in $\mathcal{G}_n$* in Section 3.1, rotations are defined in unit planes $L = \sum_{i=1}^{n} \sum_{j=i+1}^{n} k_{ij} e_i \wedge e_j$ with $0 \le k_{ij} \le 1$ and $\sum_{i,j} k_{ij} = 1$. Obviously there are $\binom{n}{2}$ such planes that can be extracted as

$$e^{\phi L} = e^{\phi_1 e_1 \wedge e_2}\, e^{\phi_2 e_1 \wedge e_3} \cdots e^{\phi_{\binom{n}{2}} e_{n-1} \wedge e_n} \; ,$$

where $\phi = \frac{\phi_1}{k_{11}} + \frac{\phi_2}{k_{12}} + \cdots + \frac{\phi_{\binom{n}{2}}}{k_{n-1\,n}}$

This means that in n dimensions two functions $\mathbf{f}_1, \mathbf{f}_2 : \mathbb{R}^n \to \mathbb{R}^m$ that differ in rotation, can finally differ in at most $\binom{n}{2}$ angles. Taking this in mind one can see, that for computing all angles, the functions $\mathbf{f}_1, \mathbf{f}_2$ must have the form $\mathbf{f}(r, \phi_1, \phi_2, \ldots, \phi_{\binom{n}{2}})$, i.e. two equal functions that differ in rotation and scale (that is equal in all dimensions), $\mathbf{f}_1(\mathbf{x}) = \mathbf{f}_2(e^{-\frac{\alpha}{2}L}\, \mathbf{x}\, e^{\frac{\alpha}{2}L})$ can be written as

$$\mathbf{f}_1(\log(r), \phi) = \mathbf{f}_2(\log(r) - \log(s), \phi - \alpha) \; , \qquad (16)$$

where $\phi = (\phi_1, \phi_2, \ldots, \phi_{\binom{n}{2}})^T$, $\alpha = (\alpha_1, \alpha_2, \ldots, \alpha_{\binom{n}{2}})^T$ and $r > 0, s > 0$. These coordinates are related to the Cartesian coordinates by

$$
\begin{pmatrix} r \\ \phi_1 \\ \phi_2 \\ \vdots \\ \phi_{\binom{n}{2}} \end{pmatrix} \;\hat{=}\; \underbrace{e^{-\frac{\phi_1}{2} e_1 \wedge e_2} \ldots e^{-\frac{\phi_{\binom{n}{2}}}{2} e_{n-1} \wedge e_n} (r e_1) e^{\frac{\phi_1}{2} e_1 \wedge e_2} \ldots e^{\frac{\phi_{\binom{n}{2}}}{2} e_{n-1} \wedge e_n}}_{\text{Cartesian}}
$$
$$(17)$$

Given equation (16), $s > 0$ and $\alpha \in \mathbb{R}^{\binom{n}{2}}$ can be computed in the same way as for shifted vector valued signals.

4.3 Translation, Rotation and Scale Invariance

Although so far the generalization was easily done by exchanging the classical Fourier-Transform by the so called Clifford-Fourier-Transform, the generalization of the registration of a rotated, scaled and shifted image is a challenging task.

Let $\mathbf{f}_1, \mathbf{f}_2 : \mathbb{R}^n \to \mathbb{R}^m$ be two multichannel images with the relation

$$\mathbf{f}_1(\mathbf{x}) = \mathbf{f}_2\left(e^{-\frac{1}{2}\phi L}\, \frac{\mathbf{x}}{s}\, e^{\frac{1}{2}\phi L} - \mathbf{t}\right) \; ,$$

with $\mathbf{t} \in \mathbb{R}^n, \phi \in \mathbb{R}^{\binom{n}{2}}$ and $s > 0$. The Fourier-Transforms of $\mathbf{f}_1$ and $\mathbf{f}_2$ have the relation

$$\mathbf{F}_1(\chi) = \mathbf{F}_2\left(e^{\frac{1}{2}\phi L} s \chi\, e^{-\frac{1}{2}\phi L}\right) \frac{e^{-2\pi i_n \chi \cdot \mathbf{t}}}{s^n} \; .$$

Getting rid of the factor $e^{-2\pi i_n \chi \cdot \mathbf{t}}$ by computing the magnitudes, would allow to compute the scale and the angles and afterwards the shift. Unfortunately this step would result in a so called scalar field, which can be imagined as a grayscaled image, i.e. from here
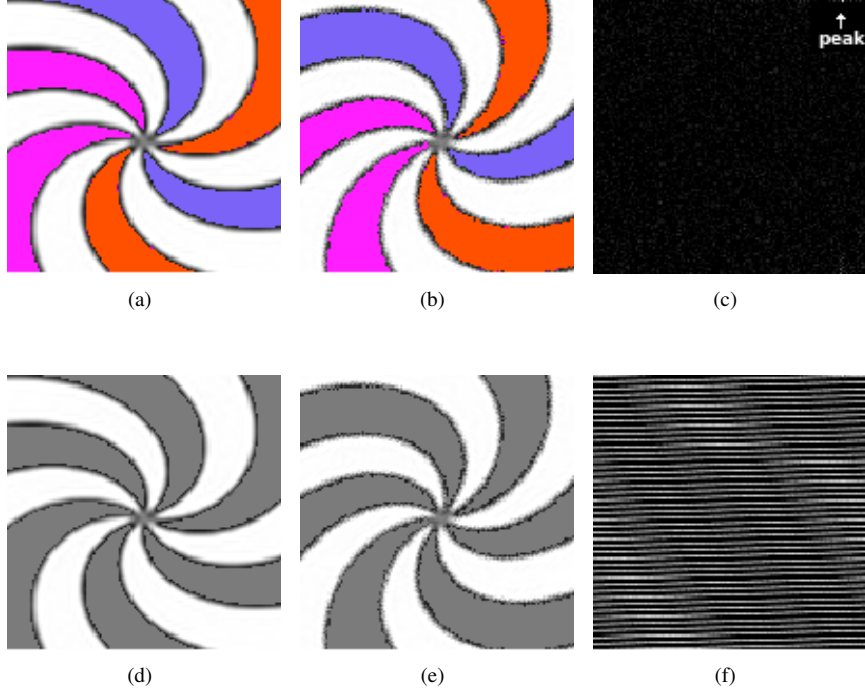
Figure 2: Images (a) and (b) are the two related color images that served as inputs for the presented multichannel registration algorithm. The result is shown in (c), a peak on the upper right. Transforming (a) and (b) into gray values (d) respective (e), the result (f) is no more a single peak, i.e. the rotation angle can not be computed anymore.

on the algorithm would operate on grayscaled and no more on multichannel images.

From equation (14) and the latter relation directly follows:

$$(-1)^{n-1}F_{1_1}(\chi)e_1 + (-1)^{n-1}F_{1_2}(\chi)e_2\cdots + (-1)^{n-1}F_{1_n}(\chi)e_n$$
$$= F_{2_1}(e^{\frac{1}{2}\phi L}\,s\chi\,e^{-\frac{1}{2}\phi L})\,\frac{e^{-2\pi i_n\chi\cdot\mathbf{t}}}{s^n}e_1$$
$$+ F_{2_2}(e^{\frac{1}{2}\phi L}\,s\chi\,e^{-\frac{1}{2}\phi L})\,\frac{e^{-2\pi i_n\chi\cdot\mathbf{t}}}{s^n}e_2$$
$$+ \cdots + F_{2_n}(e^{\frac{1}{2}\phi L}\,s\chi\,e^{-\frac{1}{2}\phi L})\,\frac{e^{-2\pi i_n\chi\cdot\mathbf{t}}}{s^n}e_n\;,$$

where F_{i_j} is the classical Fourier Transform of image i and channel j. Computing the magnitudes component wise results in

$$M_{1_1}(\chi)e_1 + M_{1_2}(\chi)e_2 + \cdots + M_{1_n}(\chi)e_n$$
$$= M_{2_1}(e^{\frac{1}{2}\phi L}\,s\chi\,e^{-\frac{1}{2}\phi L})\,\frac{e_1}{s^n} + M_{2_2}(e^{\frac{1}{2}\phi L}\,s\chi\,e^{-\frac{1}{2}\phi L})\,\frac{e_2}{s^n}$$
$$+ \cdots + M_{2_n}(e^{\frac{1}{2}\phi L}\,s\chi\,e^{-\frac{1}{2}\phi L})\,\frac{e_n}{s^n}\;,$$

or in shorthand notation

$$\mathbf{M}_{F1}(\chi) = \mathbf{M}_{F2}(e^{\frac{1}{2}\phi L}\,\frac{\chi}{s}\,e^{-\frac{1}{2}\phi L})\frac{1}{s^n}\;,$$

which can be rewritten in transformed coordinates as

$$\mathbf{M}_{F1}(\log(r),\phi) = \mathbf{M}_{F2}(\log(r)-\log(s),\phi-\alpha)\frac{1}{s^n}\;.$$

Clifford Fourier Transforming both sides leads to

$$\mathbf{F}_{M_{F1}}(\rho,\xi) = \mathbf{F}_{M_{F1}}(\rho,\xi)\frac{e^{-2\pi i_n\binom{\rho}{\xi}\cdot\binom{\log(s)}{\alpha}}}{s^n}\;.$$

From here on, computing s^n, then α and finally $\mathbf{t}$ can be done analogously to the case of grayscaled images, that was described previously.

5 EVALUATION

The evaluation of our approach was made with two different kinds of data: artificial and real world data.

An artificial color image has been created such that the different colors within the image correspond to the same gray value after conversion to grayscale (cf. Figure 2). As real world data the 30th slice of a monkey head *Positron Emission Tomography* (PET) scan (cf. Figure 3), available from [13], has been chosen.

The registration of the artificial data was done by first rotating this image by a certain degree and then registering it as described in *Rotation and Scale Invariance* of Section 4. This step shows the potential and advantages of this multichannel registration and will be discussed in the next Section.

The evaluation of the monkey head PET was similar to the afore mentioned case of the artificial data. In contrast with the artificial data, the registration was executed on each single channel (red, green and blue), on the average signal of the three channels and on the
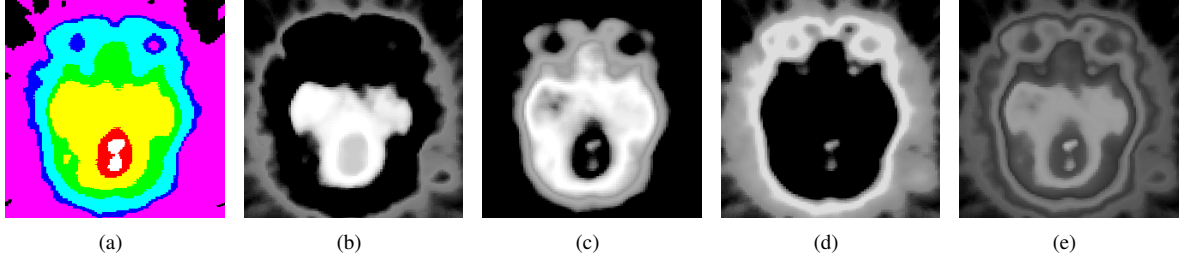
Figure 3: This images are taken from the 30th slice of a PET scan of a monkey head available from [13]. The images are respectively, the original PET image (a) itself, then the red (b), green (c) and blue (d) channels of the original image, and the average (e) of the three channels.

multichannel data itself. These steps were performed ten times to obtain many different results. Afterwards the min., max. and avg. errors were computed. As error measure we use the difference of the computed angle and the ground truth.

Since the registration on each single channel respectively on the average signal are *state of the art* approaches, this evaluation procedure compares them with the presented multichannel registration algorithm.

6 RESULTS

The basic outcome of this work is a novel approach for the registration of multichannel images, achieved by the generalization of the Fourier(-Mellin) Transform using Geometric Algebra multivectors as basis elements.

The main advantage of this algorithm is that it directly operates on the multichannel signal, instead of e.g. scaling the signal down to one dimension (e.g. by averaging) and thereby loosing a lot of information. This information loss in some cases will negatively affect on the accuracy of the registration results, as can be seen in Figure 2. Given the multichannel information, this artificially generated image is rotation invariant, i.e. the rotation relation of two different images (Figures 2(a) and (b)) is unique and can be computed with our algorithm. Computing the gray image would map all given colors, in this case, to the same gray values (Figures 2(d) and (e)), such that the computation of the angle is impossible from here on. Figures 2(c) and (f) depict the mentioned behavior of both processes, i.e. the former image shows a clearly visible peak on the upper right (the unique solution), while the latter image has got many different local maxima.

The PET images that were used for the evaluation are shown in Figure 3. Adding certain Gaussian noise ($\mu = 0$ and $\sigma^2 \in \{0, 0.1, 0.2, 0.3, 0.4, 0.5\}$) to the rotated image and subsequent performing the steps as described in the previous Section, results in the computed min., max. and avg. errors that are shown in Tables 1,2 and 3 respectively.

σ^2	ch. 1	ch. 2	ch. 3	avg.ch.	multich.
0	0.044	0.272	0.044	0.272	0.044
0.1	0.005	0.064	0.064	0.005	0.005
0.2	0.061	0.061	0.101	0.061	0.061
0.3	0.111	0.111	0.297	0.219	0.100
0.4	0.074	0.074	0.074	0.060	0.060
0.5	0.266	0.132	0.285	0.150	0.112

Table 1: min. errors

σ^2	ch. 1	ch. 2	ch. 3	avg.ch.	multich.
0	2.189	2.030	3.436	2.189	1.062
0.1	1.624	1.447	2.994	1.955	1.248
0.2	99.738	2.128	4.405	4.118	1.612
0.3	88.483	4.405	4.108	161.608	1.806
0.4	48.528	3.430	31.653	155.403	1.762
0.5	79.519	55.548	118.452	134.363	1.891

Table 2: max. errors

σ^2	ch. 1	ch. 2	ch. 3	avg.ch.	multich.
0	0.675	1.021	1.309	0.986	0.516
0.1	0.618	0.919	1.411	0.801	0.665
0.2	19.418	1.041	1.480	1.043	0.688
0.3	9.600	2.170	1.392	29.621	0.891
0.4	7.943	1.127	4.230	45.112	0.791
0.5	16.028	8.471	36.845	23.743	0.900

Table 3: avg. errors

These results show, that the registration performed on multichannel data (cf. column *multich.*) is more accurate and more stable to noise than the registration on each channel separately (cf. columns *ch. i*) or on the average of all channels (cf. column *avg.ch.*). At the same time one can see that the registration on channel 2 (blue) was far more accurate than the registration on the other single channels in the most cases, i.e. combining the results of the different channels, to compute the rotation angle, is a hard and still unsolved task. Having the multichannel registration as presented here, the solution of the mentioned task becomes no longer necessary since the registration is performed on all channels simultaneously.

7 CONCLUSION

The proposed registration algorithm is an extension of the well-known and widely used Fourier Transform which operates on scalar data (e.g. gray images). As many image sources provide multi-channel information, there is a need to process this data in an adequate way which prevents loss of information and keeps the original dimensionality of the information.

Geometric Algebra has been chosen as a mathematical framework which allows a.o. an extension of the Fourier Transform, called the Clifford Fourier Transform [6], to be able to operate on multichannel signals directly, i.e. it allows a frequency analysis on vector valued signals and an implementation of vector valued filters.

It has been shown in [6], that the Clifford Fourier Transform is a sum of many classical Fourier Transforms. As nowadays signal-processing hardware or recent graphics hardware provides interfaces to perform the Fast Fourier Transform (FFT) hardware-accelerated, it is suitable to design more complex algorithms on base of the FFT and remain in suitable computing times.

First investigation of the results shows that our registration on multichannel signals is very robust to noise, and that this approach provides potential for many applications on vector valued data.

8 FUTURE WORK

Our next steps will be a qualitative comparison with conventional approaches as well as an evaluation on volumetric image data.

Since a very high accuracy is needed, especially in the context of medical imaging, our algorithm will be extended with a spectrum based subpixel registration approach like [17], to achieve even more accurate results.

Having this, other approaches, such as the improvement of the resolution by registration [9], will be easily applicable with our multichannel registration algorithm as well.

Further, to improve performance, our future work will also include an implementation in CUDA respective OpenCL.

REFERENCES

[1] Eduardo Bayro-Corrochano and Garret Sobczyk, editors. *Geometric Algebra with Applications in Science and Engineering*. Birkhäuser, 2001.

[2] Thomas Bülow and Gerald Sommer. Hypercomplex signals-a novel extension of the analytic signal to the multidimensional case. *IEEE trans. on Signal Processing*, pages 2844–2852, 2001.

[3] Qin-Sheng Chen. *Image Registration and its Applications in Medical Imaging*. PhD thesis, Free University Brussels (VUB), 1993.

[4] Chris Doran and Anthony Lasenby. *Geometric Algebra for Physicists*. Cambridge University Press, 2003.

[5] J. Ebling and G. Scheuermann. Clifford Convolution And Pattern Matching On Vector Fields. In *Procceedings of IEEE Visualization(VIS)*, pages 193–200, 2003.

[6] Julia Ebling. Clifford fourier transform on vector fields. *IEEE Transactions on Visualization and Computer Graphics*, 11(4):469–479, 2005.

[7] Todd A. Ell and Stephen J. Sangwine. Hypercomplex fourier transforms of color images. In *in Proc. ICIP*, pages 137–140, 2001.

[8] Michael Felsberg. *Low-Level Image Processing with the Structure Multivector*. PhD thesis, Inst. f. Informatik u. Prakt. Math. der Christian-Albrechts-Universität zu Kiel, 2002.

[9] Michal Irani and Shmuel Peleg. Improving resolution by image registration. *CVGIP: Graph. Models Image Process.*, 53(3):231–239, 1991.

[10] Robert J. Marks II. *Handbook of Fourier analysis and its applications*. Oxford: Oxford University Press., 2009.

[11] Christian Perwass. *Geometric Algebra with Applications in Engineering*. Springer, 2009.

[12] D. L. Pham, C. Xu, and J. L. Prince. A survey of current methods in medical image segmentation. In *Annual Review of Biomedical Engineering*, volume 2, pages 315–338. 2000.

[13] Stefan Roettger. The erlangen volume library. http://www9.informatik.uni-erlangen.de/External/vollib/.

[14] Gustavo K. Rohde, Sinisa Pajevic, Carlo Pierpaoli, and Peter J. Basser. A comprehensive approach for multi-channel image registration. In *WBIR'03*, pages 214–223, 2003.

[15] Didier Stricker. Tracking with reference images: a real-time and markerless tracking solution for outdoor augmented reality applications. In *VAST '01: Proceedings of the 2001 conference on Virtual reality, archeology, and cultural heritage*, pages 77–82, New York, NY, USA, 2001. ACM.

[16] Richard Szeliski. Image alignment and stitching: a tutorial. *Found. Trends. Comput. Graph. Vis.*, 2(1):1–104, 2006.

[17] K. Takita, T. Aoki, Y. Sasaki, T. Higuchi, and K. Kobayashi. High-accuracy subpixel image registration based on phase-only correlation. In *IEICE Trans. Fund.*, volume E86-A, no. 8, pages 1925–1934, 2003.

[18] John A. Vince. *Geometric Algebra for Computer Graphics*. Springer, 1 edition, 4 2008.

[19] B. Zitova. Image registration methods: a survey. *Image and Vision Computing*, 21(11):977–1000, October 2003.

A MATHEMATICAL PROOFS

A.1 Proof of (1)

$$(e_i \wedge e_j)(e_i \wedge e_j) = (-e_j \wedge e_i)(e_i \wedge e_j)$$
$$= (-e_j e_i)(e_i e_j)$$
$$= -e_j \underbrace{e_i e_i}_{1} e_j$$
$$= -\underbrace{e_j e_j}_{1}$$
$$= -1$$

q.e.d.

A.2 Proof of (4)

$$e^{-\frac{\phi}{2}e_1 \wedge e_2} e_3 e^{\frac{\phi}{2}e_1 \wedge e_2}$$
$$= (\cos(\frac{\phi}{2}) - (e_1 \wedge e_2)\sin(\frac{\phi}{2})) e_3 (\cos(\frac{\phi}{2}) + (e_1 \wedge e_2)\sin(\frac{\phi}{2}))$$
$$= (\cos(\frac{\phi}{2}) - (e_1 \wedge e_2)\sin(\frac{\phi}{2}))(\cos(\frac{\phi}{2}) + (e_1 \wedge e_2)\sin(\frac{\phi}{2})) e_3$$
$$= (\cos(\frac{\phi}{2})^2 + \sin(\frac{\phi}{2})^2) e_3$$
$$= e_3$$

q.e.d.

A.3 Proof of (15)

Let $\mathbf{f} : \mathbb{R}^n \to \mathcal{G}_n$ be a (multi-)vector valued function, then the Clifford-Fourier-Transform of $\mathbf{f}(\mathbf{x} - \mathbf{t})$ equals

$$\mathbf{F}_t(\mathbf{u}) = \int_{\mathbb{R}^n} \mathbf{f}(\mathbf{x} - \mathbf{t}) e^{-2\pi i \mathbf{u} \cdot \mathbf{x}} \mathrm{d}\mathbf{x}$$
$$= \int_{\mathbb{R}^n} \mathbf{f}(\hat{\mathbf{x}}) e^{-2\pi i_n \mathbf{u} \cdot (\hat{\mathbf{x}} + \mathbf{t})} \mathrm{d}\hat{\mathbf{x}}$$
$$= \int_{\mathbb{R}^n} \mathbf{f}(\hat{\mathbf{x}}) e^{-2\pi i_n \mathbf{u} \cdot \hat{\mathbf{x}}} \mathrm{d}\hat{\mathbf{x}} \, e^{-2\pi i_n \mathbf{u} \mathbf{t}}$$
$$= \mathbf{F}(\mathbf{u}) \, e^{-2\pi i_n \mathbf{u} \mathbf{t}}$$

where $\mathbf{F}$ is the Fourier Transform of $\mathbf{f}$ (providing that the Fourier-Transform exists).

Now let $\mathbf{f}_1, \mathbf{f}_2 : \mathbb{R}^n \to \mathcal{G}_n$ be two (multi-)vector valued functions, such that $\mathbf{f}_1(\mathbf{x}) = \mathbf{f}_2(\mathbf{x} - \mathbf{t})$. Let $\mathbf{F}_1, \mathbf{F}_2, \mathbf{F}_t$ be the Fourier-Transforms of $\mathbf{f}_1(\mathbf{x}), \mathbf{f}_2(\mathbf{x})$ and $\mathbf{f}_2(\mathbf{x} - \mathbf{t})$, respectively, then

$$\mathbf{F}_1(\mathbf{u}) = \mathbf{F}_t(\mathbf{u})$$
$$= \mathbf{F}_2(\mathbf{u}) \, e^{-2\pi i_n \mathbf{u} \cdot \mathbf{t}}$$

q.e.d.

A.4 Proof of Dirac Delta CFT

Let $\delta : \mathbb{R}^n \to \{0, +\infty\}$ be a Dirac Delta function, defined as

$$\delta(\mathbf{x}) = \begin{cases} +\infty & , \mathbf{x} = \begin{pmatrix} 0 \\ \vdots \\ 0 \end{pmatrix} \\ 0 & , \text{else} \end{cases}$$

then the Clifford Fourier Transform of $\delta(\mathbf{x} - \mathbf{t})$ is

$$\mathbf{F}(\mathbf{u}) = \int_{\mathbb{R}^n} \delta(\mathbf{x} - \mathbf{t}) e^{-2\pi i_n \mathbf{x} \cdot \mathbf{u}} \mathrm{d}\mathbf{x}$$
$$= \int_{\mathbb{R}^n} \delta(\hat{\mathbf{x}}) e^{-2\pi i_n (\hat{\mathbf{x}} + \mathbf{t}) \cdot \mathbf{u}} \mathrm{d}\hat{\mathbf{x}}$$
$$= \int_{\mathbb{R}^n} \delta(\hat{\mathbf{x}}) e^{-2\pi i_n \hat{\mathbf{x}} \cdot \mathbf{u}} \mathrm{d}\hat{\mathbf{x}} \, e^{-2\pi i_n \mathbf{t} \cdot \mathbf{u}}$$
$$= e^{-2\pi i_n \mathbf{t} \cdot \mathbf{u}}$$

q.e.d.